Modeling and Simulation of Emissivity of Silicon-Related Materials and Structures

N.M. RAVINDRA,[1,5] KRSHNA RAVINDRA,[1,2] SUNDARESH MAHENDRA,[1,3] BHUSHAN SOPORI,[4] and ANTHONY T. FIORY[1]

1.—Department of Physics, New Jersey Institute of Technology, Newark, NJ 07102. 2.—Intern at NJIT from Union County Magnet High School, Scotch Plains, NJ 07076. 3.—Intern at NJIT from Millburn High School, Millburn, NJ 07041. 4.—National Renewable Energy Laboratory, Golden, CO 80401. 5.—E-mail: ravindra@njit.edu

A brief review of the models that have been proposed in the literature to simulate the emissivity of silicon-related materials and structures is presented. The models discussed in this paper include ray tracing, numerical, phenomenological, and semi-quantitative approaches. A semi-empirical model, known as Multi-Rad, based on the matrix method of multilayers is used to evaluate the reflectance, transmittance, and emittance for Si, SiO_2/Si, Si_3N_4/SiO_2/Si/SiO_2/Si_3N_4 (Hotliner), and separation by implantation of oxygen (SIMOX) wafers. The influence of doping concentration and dopant type as well as the effect of the angle of incidence on the radiative properties of silicon is examined. The results of these simulations lead to the following conclusions: (1) at least within the limitations of the Multi-Rad model, near the absorption edge, the radiative properties of Si are not affected significantly by the angle of incidence unless the angle is very steep; (2) at low temperatures, the emissivity of silicon shows complex structure as a function of wavelength; (3) for SiO_2/Si, changes in emissivity are dominated by substrate effects; (4) Hotliner has peak transmittance at 1.25 μm, and its emissivity is almost temperature independent; and (5) SIMOX exhibits significant changes in emissivity in the wavelength range of 1–20 μm.

Key words: Si, emissivity, Hotliner, SIMOX

INTRODUCTION

Emissivity of semiconductors plays an important role in radiation thermometry and radiative heat transfer during thermal processing. The detailed understanding of emissivity is critical for monitoring and controlling temperature in semiconductor processing techniques, such as rapid thermal processing (RTP), molecular beam epitaxy (MBE), and chemical vapor deposition (CVD). Emissivity, ε, is defined as the ratio of the radiance of a given object to that of a blackbody at the same temperature and for the same spectral and directional conditions. It is a function of surface morphology,[1,2] impurity concentration,[3] wavelength, temperature, and the presence of overlayers.[4] It is a property that must be known for accurate temperature determination of an object by measurement of its emitted electromagnetic radiation with a radiation thermometer.

Historically, the ability to model emissivity of semiconductor materials and structures has been hampered by the limited reliable data of the optical properties in the infrared (IR) range of wavelengths[5] in the literature. Even for well-understood materials, such as silicon, the data of the extinction coefficient, k, is limited, especially, for high temperatures. Ray tracing, numerical, and semi-quantitative approaches to model emissivity of silicon have been reasonably successful.

RAY TRACING TECHNIQUE

PV Optics is an optical modeling software developed by Sopori et al. at the National Renewable Energy Laboratory (Golden, CO). This software was originally developed for design and analysis of solar cells. It can calculate a variety of optical parameters

(Received May 30, 2003; accepted July 1, 2003)

for multilayer devices and is capable of handling planar as well as nonplanar interfaces. We have recently extended this package to calculate ε for samples with any surface conditions and with thin dielectric and metal layers.[6] The calculated parameters include reflectance, transmittance, and absorbance of photons in each layer and their absorption profiles. Because emissivity relates to the total absorption in the device (Eq. 3), this package can be appropriately modified to calculate emissivity. The modifications include (1) extending the wavelength range to that used in pyrometry and RTP applications and (2) including a suitable approach for calculating values of the index of refraction, n, and k corresponding to Si at different temperatures and with different material parameters. The model is used to calculate net reflectance, transmittance, and absorbance of a wafer, corresponding to light incidence from the desired surface. These data are then used to determine ε of that surface of the wafer.

Figure 1 is a schematic illustrating the methodology of performing these calculations. A beam of unit intensity is incident on the sample that has an arbitrary surface morphology. The beam is split into a large number of beamlets that impinge on a small region of the surface. Each beamlet is allowed to propagate within the sample, and its entire path is monitored while it undergoes reflection, transmission, and absorption.

The following set of equations are applied to calculate optical parameters in the bulk and to determine the effects of multilayer coatings. In the semiconductor, the beam propagates in the z direction as

$$I_{final} = I_{initial} \cdot e^{-\alpha z} \quad (1)$$

where

$$\alpha = \frac{4\pi k}{\lambda}$$

and the extinction coefficient, k, is the imaginary part of the complex refractive index

$$n(\lambda) = n - i \cdot k$$

At each interface, we use the following equations:

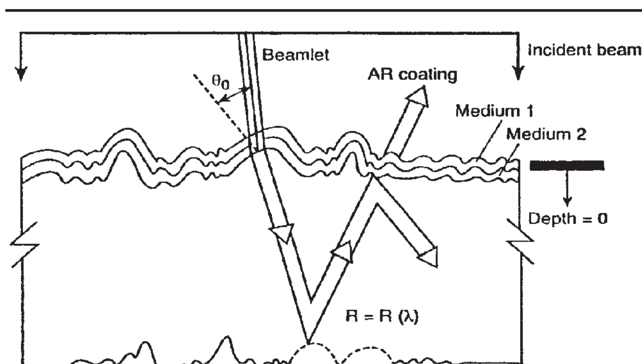

Fig. 1. A schematic illustrating the methodology of performing ray-tracing calculations.

$$\cos(\theta_0) = \hat{r}_i \cdot \hat{n} \quad (2)$$

$$\cos(\theta_j) = \sqrt{1 - (\frac{n_{j-1}}{n_j})^2 \cdot (1 - \cos(\theta_{j-1})^2)} \quad j = 1, 2, 3 \quad (3)$$

where r_i is a unit vector along the beamlet. The reflection coefficients for parallel and perpendicular polarization are

$$r_{\perp} = \frac{r_{1\perp} + A_{\perp} \cdot e^{-i\frac{4\pi}{\lambda} n_1 t_1 \cos(\theta_1)}}{1 + r_{1\perp} \cdot A_{\perp} \cdot e^{-i\frac{4\pi}{\lambda} n_1 t_1 \cos(\theta_1)}}$$

$$r_{\parallel} = \frac{r_{1\parallel} + A_{\parallel} \cdot e^{-i\frac{4\pi}{\lambda} n_1 t_1 \cos(\theta_1)}}{1 + r_{1\parallel} \cdot A_{\parallel} \cdot e^{-i\frac{4\pi}{\lambda} n_1 t_1 \cos(\theta_1)}} \quad (4)$$

where

$$A_{\perp} = \frac{r_{2\perp} + r_{3\perp} \cdot e^{-i\frac{4\pi}{\lambda} n_2 t_2 \cos(\theta_2)}}{1 + r_{2\perp} \cdot r_{3\perp} \cdot e^{-i\frac{4\pi}{\lambda} n_2 t_2 \cos(\theta_2)}}$$

$$A_{\parallel} = \frac{r_{2\parallel} + r_{3\parallel} \cdot e^{-i\frac{4\pi}{\lambda} n_2 t_2 \cos(\theta_2)}}{1 + r_{2\parallel} \cdot r_{3\parallel} \cdot e^{-i\frac{4\pi}{\lambda} n_2 t_2 \cos(\theta_2)}}$$

$$r_{j\perp} = \frac{n_{j-1} \cdot \cos(\theta_{j-1}) - n_j \cdot \cos(\theta_j)}{n_{j-1} \cdot \cos(\theta_{j-1}) + n_j \cdot \cos(\theta_j)}$$

$$r_{j\parallel} = \frac{n_{j-1} \cdot \cos(\theta_j) - n_j \cdot \cos(\theta_{j-1})}{n_{j-1} \cdot \cos(\theta_j) + n_j \cdot \cos(\theta_{j-1})}$$

In this manner, each beamlet bounces back and forth within the sample. The net energy absorbed at each plane within the sample is determined. This procedure is continued for each beamlet until the energy in the beam is reduced nearly to zero. This process yields the net reflection, transmission, and absorption in the wafer.

Thus, the model calculates total absorption, reflection, and transmission that includes the scattering effects arising from nonplanar surfaces. Because of the fact that the hemispherical emissivity is equal to the total absorption, the emissivity of each surface of the sample as a function of wavelength is determined. In addition, PV Optics can handle nonplanar surfaces.

Sato[7] has performed the first detailed measurements of temperature-dependent spectral emissivity of silicon. Using a spectrophotometer, Sato measured the emissivity (ε) of comparatively pure (resistivity ρ = 15 Ω-cm at 300 K) and heavily phosphorous-doped (ρ = 7 × 10^{-3} Ω-cm at 300 K) silicon in the temperature range of 543–1,073 K and in the spectral region from visible to 15 μm. Sato's measurements show that ε increases with increasing temperature for pure silicon in the 2–15 μm region. For n-type silicon, ε decreases with

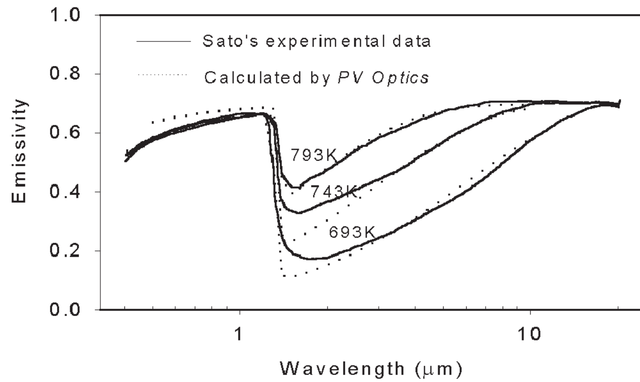

Fig. 2. A comparison of the calculated and experimental values of ε for a double-sided polished Si sample. The experimental data is from Ref. 7.

increasing temperature. In general, for silicon, the high ε in the visible region can be attributed to band-to-band transitions. For low temperatures, Si is transparent for wavelength λ greater than 1.2 μm, leading to low emissivity in near IR. For $\lambda > 6$ μm, the high ε of Si is due to lattice vibrations. For temperatures at or above 570 K, Si becomes intrinsic, leading to contribution to ε by free carriers. For temperatures greater than 870 K, ε is constant in the entire IR region. While Sato's results are very important and fundamental indeed, these results are for specific resistivities and thicknesses of the silicon wafer. In addition to the need for a generalized and detailed study of ε, a numerical model for the wavelength dependence of ε of Si would be very useful.

In Fig. 2, a comparison of the results of Sato is made with that obtained using PV Optics. As can be seen in the figure, PV Optics yields wavelength and temperature-dependent emissivity that are in accord with the experimental results of Sato.

NUMERICAL MODEL

Using a spectral emissometer that can simultaneously measure reflectance, transmittance, and temperature, we have determined experimentally the wavelength and temperature-dependent emissivity of silicon-related materials and structures.[1,3,4] Our results of the temperature-dependent emissivity of silicon lead us to a numerical model[8] that represents the best fit to experimental data. The results are expressed empirically by the expression:

$$\varepsilon(\lambda,T) = A_0 + (A_1/\lambda) + (A_2/\lambda^2) \tag{5}$$

where

$$A_0 = 0.64362 + (0.1264 * 10^{-3})T - (0.67955 * 10^{-7})T^2$$

$$A_1 = 0.66789 - (0.1506 * 10^{-2})T + (0.65442 * 10^{-6})T^2$$

$$A_2 = -1.2978 + (0.30243 * 10^{-2})T - (0.15119 * 10^{-5})T^2$$

The term λ is the wavelength in microns, and T is the temperature in Kelvin. The results of the calculations of ε of Si as a function of λ for temperatures

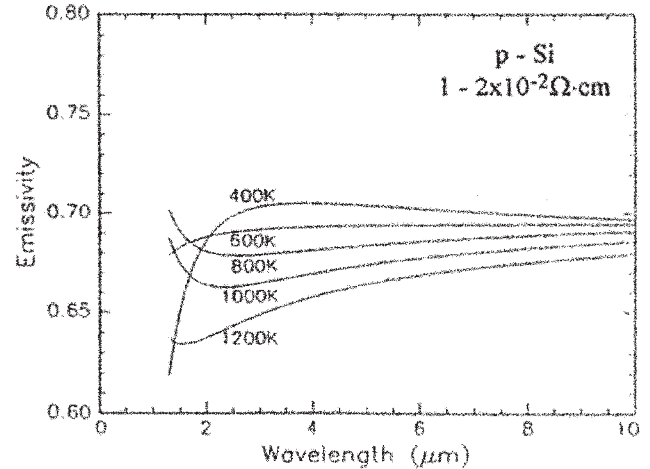

Fig. 3. The calculated emissivity for p-Si.[8]

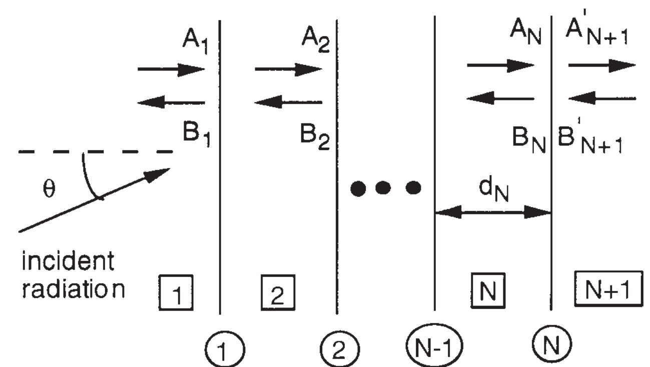

Fig. 4. A notation for the matrix method of multilayers.[10]

in the range of 400–1,200 K, based on the preceding equations, are presented in Fig. 3. As can be seen in this figure, below 2 μm, ε is highly sensitive to temperature because of bandgap and free-carrier absorption mechanisms. Above 2 μm, ε increases with temperature irrespective of λ. The calculated values of ε of Si in Fig. 3 are in accord with expectations.

MULTI-RAD

This program, developed at the Massachusetts Institute of Technology (Cambridge, MA),[9–11] can perform calculations of the radiative properties of silicon-related materials and multilayer structures. It predicts the reflectance and transmittance of a multilayer stack for a given wavelength and angle of incidence. Radiation at a given wavelength is treated as coherent, so interference effects are taken into account. The main assumptions of the theory are that the layers are parallel and optically isotropic; the surface is optically smooth; and the area in question is much larger than the wavelength of incident radiation.

A generic layered structure is shown in Fig. 4. There are N layer interfaces (circled) and N+1 "layers" (squared), including the unbounded transparent media on each side of the actual stack. The terms A_i

and B_i are the amplitudes of the forward and backward propagating electric-field vectors on the left side of the interface, i. The prime notation on A'_{N+1} and B'_{N+1} indicates that these are the amplitudes on the right side of interface N. Light is incident on interface 1, with an angle of incidence $\theta = \theta_1$.

The central equation of the multilayer theory relates the amplitudes on the left side of interface 1 with those on the right side of interface N:

$$\begin{pmatrix} A_1 \\ B_1 \end{pmatrix} = \left[\prod_{i=1}^{N} P_i D_i^{-1} D_{i+1}\right] \begin{bmatrix} A'_{N+1} \\ B'_{N+1} \end{bmatrix} = \begin{bmatrix} m_{11} & m_{12} \\ m_{21} & m_{22} \end{bmatrix} \begin{bmatrix} A'_{N+1} \\ B'_{N+1} \end{bmatrix} \quad (6)$$

where P_i is the propagation matrix, D_i is the dynamical matrix, and m_{ij} is an element of the transfer function matrix. The propagation matrix accounts for the effect of absorption and interference within a layer i bounded by two interfaces. Because layer 1 is not bound by two interfaces, the propagation matrix has no meaning, and P_1 is set equal to the identity matrix. For layers 2, 3, …, N, the propagation matrix is

$$P_i = \begin{bmatrix} e^{i\phi_i} & 0 \\ 0 & e^{-i\phi_i} \end{bmatrix} \quad (7)$$

where $\phi_i = 2\pi\bar{n}_i d_i \cos\bar{\theta}_i/\lambda$ is the phase shift. The complex refractive index is $\bar{n}_i = n_i + i\kappa_i$, where n is the refractive index, and κ is the extinction coefficient. In this model, it is assumed that the bounding media are in vacuum, with a refractive index of 1. The thickness of the layer is d; $\bar{\theta}_i$ is the complex angle; and λ is the wavelength of the incident wave in vacuum.

The dynamical matrix accounts for reflection and refraction at the interface i, relating amplitudes of the reflected and refracted waves on either side of the interface. Depending on the state of polarization of the wave, the dynamical matrix is given by

$$D_i = \begin{pmatrix} 1 & 1 \\ \bar{n}_i\cos\bar{\theta}_i & -\bar{n}_i\cos\bar{\theta}_i \end{pmatrix} \text{s wave} \quad (8)$$

$$D_i = \begin{pmatrix} \cos\bar{\theta}_i & \cos\bar{\theta}_i \\ \bar{n}_i & -\bar{n}_i \end{pmatrix} \text{p wave} \quad (9)$$

where s and p indicate that the electric-field vector is perpendicular and parallel to the plane of incidence, respectively. Nonabsorbing layers have purely real refractive indices, so they have purely real angles that can be interpreted as the direction of propagation in the layer. Absorbing layers have complex refractive indices, resulting in complex angles that have no direct physical interpretation. The angle θ_1 is purely real and interpreted as the angle of incidence. Given the angle of incidence, the complex angles for the other layers are calculated in succession using the complex form of Snell's law:

$$\sin\bar{\theta}_{i+1} = \frac{\bar{n}_i}{\bar{n}_{i+1}}\sin\bar{\theta}_i \quad (10)$$

The reflectance for a s or p wave for the entire stack is the ratio of the intensities of the forward and backward propagating waves on the left side of interface 1. The transmittance for a s or p wave is the ratio of the intensities of the forward propagating wave on the right side of interface N and the forward propagating wave on the left side of interface 1. The intensity of an electromagnetic wave is proportional to the square of its amplitude. Thus,

$$R_{s/p} = \frac{B_1}{A_1} = \left|\frac{m_{21}}{m_{11}}\right|^2 \quad (11)$$

$$T_{s/p} = \frac{\bar{n}_{N+1}\cos\theta_{N+1}}{\bar{n}_1\cos\theta_1}\frac{A'_{N+1}}{A_1} = \frac{\bar{n}_{N+1}\cos\theta_{N+1}}{\bar{n}_1\cos\theta_1}\left|\frac{m_{21}}{m_{11}}\right|^2 \quad (12)$$

Thermal radiation is usually well approximated as unpolarized, in which case, the spectral directional reflectance and transmittance, $R_{\lambda,\theta}$ and $T_{\lambda,\theta}$, may be calculated as a simple arithmetic average of the s- and p-wave properties.[10]

The spectral directional absorptance is calculated by subtracting the reflectance and transmittance from unity, and the spectral directional emittance is calculated by assuming Kirchhoff's law on a spectral basis:

$$\alpha_{\lambda,\theta} = \varepsilon_{\lambda,\theta} = 1 - R_{\lambda,\theta} - T_{\lambda,\theta} \quad (13)$$

where the subscripts λ and θ have been introduced to indicate spectral and directional properties, respectively. Kirchhoff's law on a spectral basis is valid if the emitting object is in local thermodynamic equilibrium, i.e., a single temperature can characterize it. If there is a significant temperature gradient in the part of the wafer that is emitting or if the phonons and electrons are not in thermal equilibrium (e.g., laser annealing), then Kirchhoff's law becomes invalid. In most RTP processes, neither of these conditions is encountered for a silicon wafer.

To obtain the hemispherical spectral properties, integration over all directions in the hemisphere is performed. The matrix method of multilayers described previously makes the assumption that there is no variation of the radiative properties with the azimuthal angle. The spectral absorptance integrated over a particular range of angle of incidence, defined by θ_{min} and θ_{max}, is given by

$$\alpha_\lambda = \frac{\int_{\theta_{min}}^{\theta_{max}} \alpha_{\lambda,\theta}\cos\theta\sin\theta\, d\theta}{\frac{1}{2}\sin^2\theta_{max} - \sin^2\theta_{min}} \quad (14)$$

where θ is the angle of incidence. The expression is analogous for emittance, reflectance, and transmittance.

In Figs. 5 and 6, the simulated radiative properties of lightly doped, 700-µm-thick n-Si is plotted as a function of angle of incidence for $\lambda = 0.9$ µm and $\lambda = 2.7$ µm, respectively. As can be seen in these

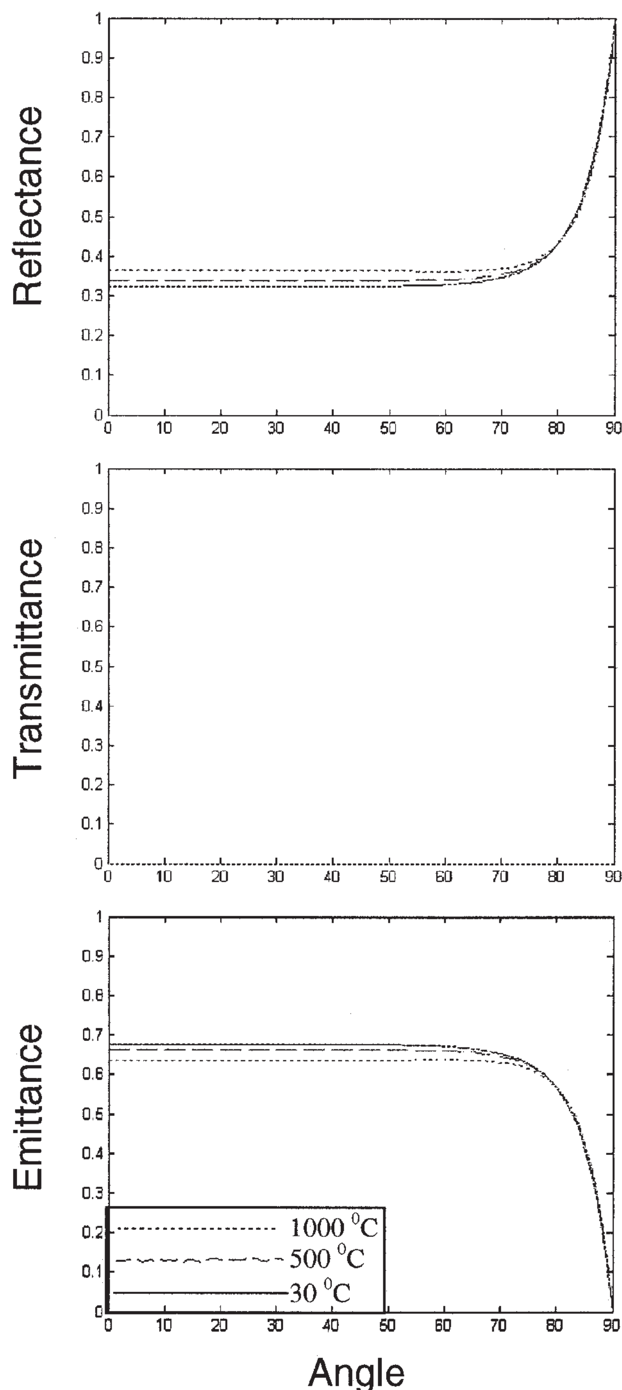

Fig. 5. The simulated radiative properties of 700-μm-thick n-Si as a function of the angle of incidence for λ = 0.9 μm. Wafer resistivity = 0.523 Ω-cm.

figures, the change in emissivity with the angle of incidence is very small from 0° to 70°. The emissivity changes significantly beyond 70°. This is once again illustrated in Fig. 7 for three specific temperatures. At high temperatures, the emissivity of silicon reaches its intrinsic value of 0.7 and remains independent of wavelength in the 1–20-μm range. At shorter wavelengths, close to the absorption edge of silicon, the transmittance is negligible. However, for λ = 2.7 μm, the transmittance becomes significant, as can be seen in Fig. 6. At high temperatures, transmittance becomes negligible. At low temperatures, the emissivity of silicon is a complex function of wavelength, as can be seen in Fig. 7. A detailed analysis of Sato's data and comparison with the results from the Multi-Rad model has been discussed elsewhere.[12]

The simulated emissivity of SiO_2/700-μm Si is shown in Fig. 8 for varying oxide thickness for three specific temperatures. A comparison of Figs. 7 and 8 shows that the change in emissivity with wavelength is determined by the spectral properties of the substrate material—silicon. At least in the thickness range of 1–100 nm, considered in the simulations in Fig. 8, the influence of SiO_2 films on the emissivity can be noticed in the wavelength range of 8–10 μm.

There have been several attempts to formulate methodologies that can lead to wafer emissivity-independent, temperature measurements in RTP. One of these approaches uses a Hotliner. The Hotliner is comprised of a heavily doped, p-silicon substrate clad with Si_3N_4/SiO_2 films on both sides. In Fig. 9, the simulated radiative properties of Hotliner (57-nm Si_3N_4/25-nm SiO_2/700-μm p-silicon/25-nm SiO_2/57-nm Si_3N_4) is presented, as a function of wavenumber, for three specific temperatures. As can be seen in this figure, the Hotliner is characterized by an extremely weak transmittance (note the scale on the Y-axis in the transmittance spectra in Fig. 9), and its change in emissivity with temperature is weak (varying by several percent).

Silicon-on-insulator is the preferred substrate for low-power, high-speed microelectronic devices.[13] One of the well-accepted methods of fabricating silicon-on-insulator is by separation by implantation of oxygen (SIMOX). In both the SIMOX and Smart-Cut processes, the wafer temperature must be kept at 600°C for long durations to implant a sufficiently high dose of oxygen or hydrogen. Thus, the need to monitor process temperature is of fundamental importance not only during the subsequent processing of these wafers for device fabrication but also for manufacturing the wafers. In spite of SIMOX being a mature technology, it represents a challenge for appropriate choice of wavelengths for pyrometry because of the complexity of the built-in multilayers and the interfaces. In Figs. 10 and 11, the simulated radiative properties of SIMOX are plotted for two oxide thicknesses. As can be seen in these figures, SIMOX exhibits large variations in the radiative properties in the wavelength range of 1–10 μm. While the buried oxide thickness has some influence on the radiative properties of SIMOX, its reflectance is very high compared to bare silicon. The emissivity is a complex function of wavelength even at high temperatures. At shorter wavelengths, SIMOX exhibits low emissivities. Significant changes in emissivity become noticeable in the 4–8-μm wavelength range.

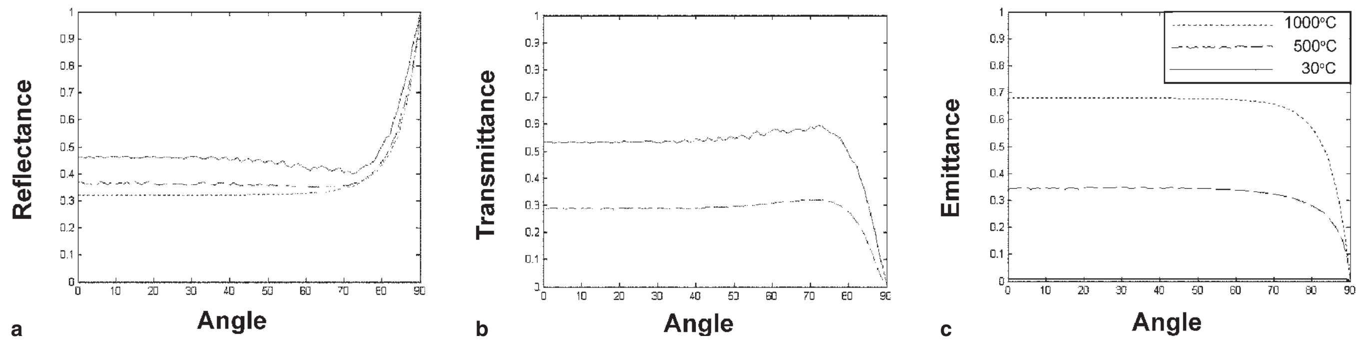

Fig. 6. The simulated radiative properties of 700-μm-thick n-Si as a function of angle for $\lambda = 2.7$ μm. Wafer resistivity = 0.523 Ω-cm.

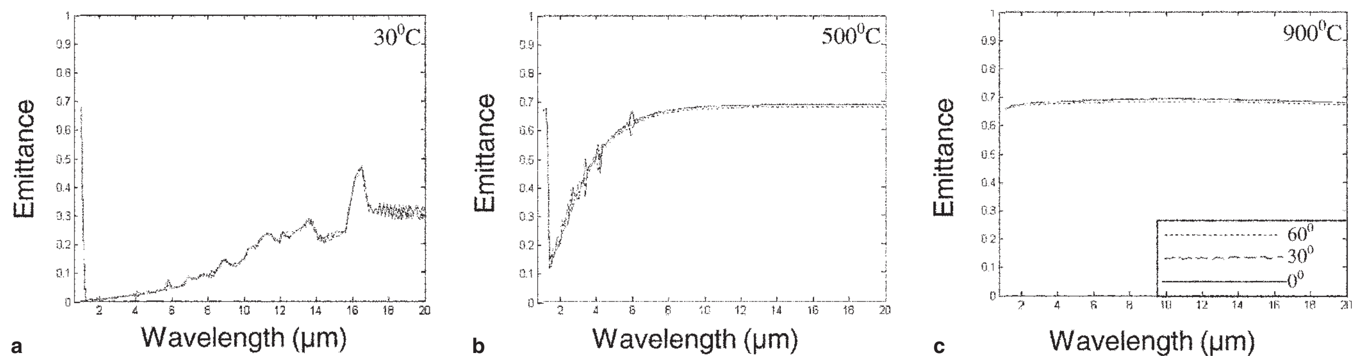

Fig. 7. The simulated emissivity of n-type Si at varying temperatures and angles of incidence. The wafer is 700-μm thick and has a resistivity of 0.523 Ω-cm.

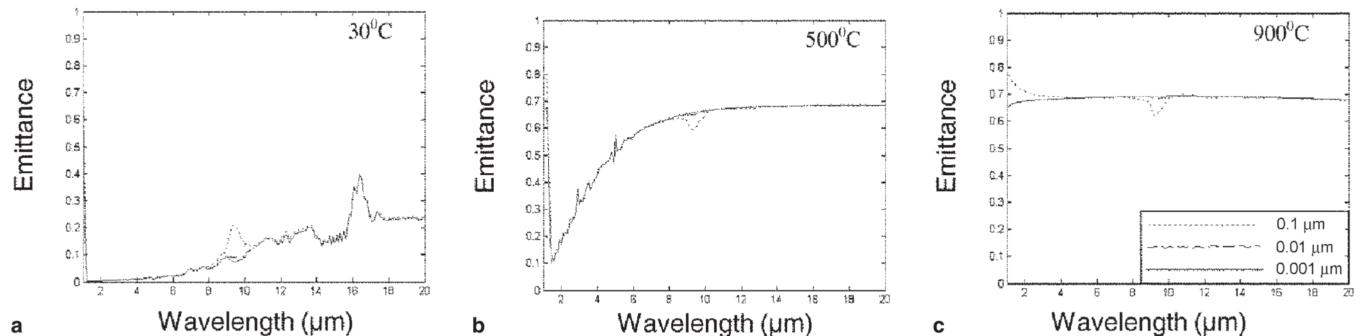

Fig. 8. The simulated emissivity of SiO_2/700-μm Si. The SiO_2 thickness is displayed in the legend.

CONCLUSIONS

A brief review of the modeling and simulation approaches to understanding the radiative properties of silicon-related materials and structures has been presented in this study. Semi-empirical models, such as the ray tracing technique, Multi-Rad, and numerical approaches have been discussed. Simulations of the radiative properties have been performed for silicon substrates as function of angle of incidence, SiO_2/Si for varying oxide thickness, Hotliner (57-nm Si_3N_4/25-nm SiO_2/700-μm p-silicon/25-nm SiO_2/57-nm Si_3N_4), and SIMOX. In the range of 0–70°, emissivity does not change with the angle of incidence. The emissivity spectra of SiO_2/Si are dominated by the radiative properties of the silicon substrate. Hotliner exhibits an emissivity that is insensitive to temperature and wavelength. Simulations of SIMOX reveal high reflectivity accompanied by low emissivity at short wavelengths.

ACKNOWLEDGEMENTS

The work presented in this paper was partially supported by SEMATECH, the U.S. Department of Defense, DARPA, and the U.S. Department of Energy at various stages of the project. The authors are thankful to a number of industrial collaborators including Advanced Fuel Research, Advanced Micro Devices, Applied Materials, Bell Laboratories, IBM, Intel, Lucent Technologies, and Steag-AST Electronik.

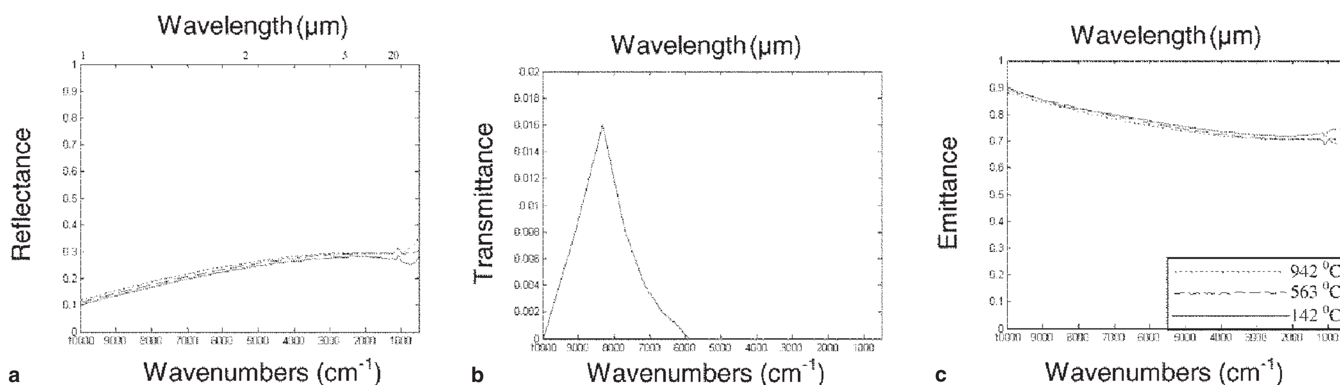

Fig. 9. The simulated radiative properties of Hotliner (57-nm Si_3N_4/25-nm SiO_2/700-µm p-silicon/25-nm SiO_2/57-nm Si_3N_4) as a function of wavenumber.

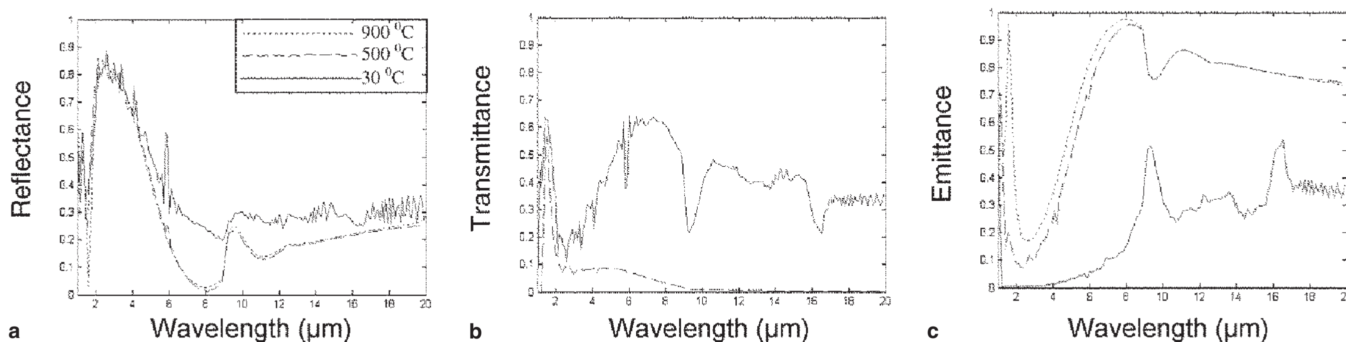

Fig. 10. The simulated radiative properties of SIMOX (200-nm Si/400-nm SiO_2/700-µm p-Si).

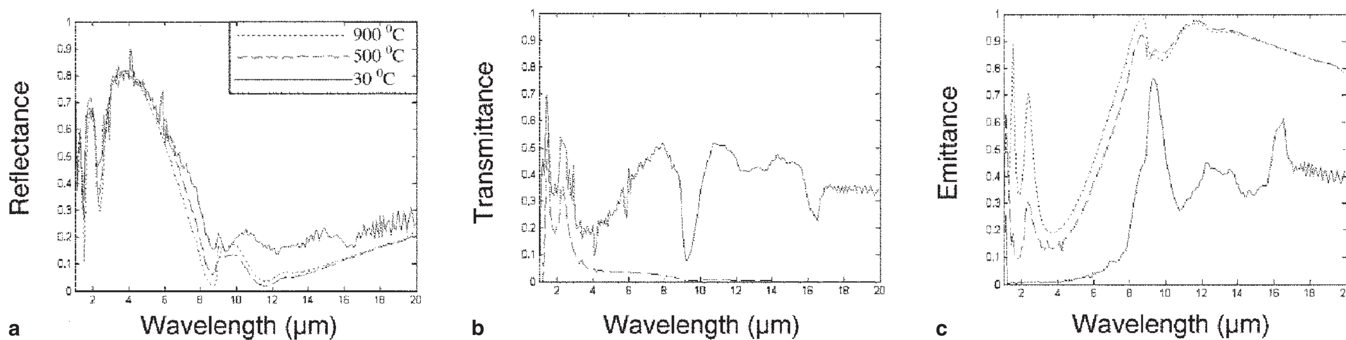

Fig. 11. The simulated radiative properties of SIMOX with twice the oxide thickness of Fig. 10 (200-nm Si/800-nm SiO_2/700-µm p-Si).

REFERENCES

1. S. Abedrabbo, J.C. Hensel, A.T. Fiory, B. Sopori, W. Chen, and N.M. Ravindra, *Mater. Sci. Semicond. Process.* 1, 187 (1998).
2. P. Vandenabeele and K. Maex, *J. Appl. Phys*. 72, 5867 (1992).
3. N.M. Ravindra, S. Abedrabbo, W. Chen, F.M. Tong, A.K. Nanda, and A.C. Speranza, *IEEE Trans. Semicond. Manuf.* 11, 30 (1998).
4. N.M. Ravindra, S. Abedrabbo, O.H. Gokce, F.M. Tong, A. Patel, R. Velagapudi, G.D. Williiamson, and W.P. Maszara, *IEEE Trans. Comp., Packag. Manuf. Technol., Part A* 21, 441 (1998).
5. H.R. Phillip, *Handbook of Optical Constants of Solids*, ed. E.D. Palik (Orlando, FL: Academic Press, 1985).
6. B. Sopori, W. Chen, J. Madjdpour, and N.M. Ravindra, *J. Electron. Mater.* 28, 1385 (1999).
7. K. Sato, *Jpn. J. Appl. Phys.* 6, 339 (1967).
8. N.M. Ravindra, W. Chen, F.M. Tong, and A. Nanda, *Transient Thermal Processing Techniques in Electronic Materials*, eds. N.M. Ravindra and R.K. Singh (Warrendale, PA: TMS, 1996).
9. P. Yeh, *Optical Waves in Layered Media* (New York: Wiley, 1988), ch. 5.
10. J.P. Hebb and K.F. Jensen, *J. Electrochem. Soc.* 143, 1142 (1996).
11. R. Siegel and J.R. Howell, *Thermal Radiation Heat Transfer* (Washington, D.C.: Hemisphere Publishing Corporation, 1992).
12. N.M. Ravindra, B. Sopori, O.H. Gokce, S.X. Cheng, A. Shenoy, L. Jin, S. Abedrabbo, W. Chen, and Y. Zhang, *Int. J. Thermophys.* 22, 1593 (2001).
13. S.S.K. Iyer, X. Lu, J.B. Liu, J. Min, Z.N. Fan, P.K. Chu, C.M. Hu, and N.W. Cheung, *IEEE Trans. Plasma Sci.* 25, 1128 (1997).